to be rather sensitive to slight changes in the constituents of the complex that are rather distant from the metal atom primarily concerned with the change of spin state. Thus changes in the counterion[17] and in ligand substituents[16] may drastically alter the character of the observed Mössbauer spectra. The exact origin of these effects, whether electronic, steric, or other in nature, is not known with certainty.

As far as iron nitrosyl complexes are concerned, the only reported example of a rapid $S = {}^3/_2 - {}^1/_2$ spin-state transition is [Fe(TMC)NO]$(BF_4)_2$ where TMC = 1,4,8,11-tetramethyl-1,4,8,11-tetraazacyclotetradecane (tetramethylcyclam).[18] However, this compound exhibits Mössbauer parameters considerably different from those of [Fe(salphen)NO]. Thus at 300 K, the quadrupole splitting and the isomer shift of [Fe(TMC)NO]$(BF_4)_2$ have been reported as $\Delta E_Q = 0.53$ mm s^{-1} and $\delta^{IS} = +0.46$ mm s^{-1}, respectively, whereas at 10 K, the values $\Delta E_Q = 0.645$ mm s^{-1} and $\delta^{IS} = +0.588$ mm s^{-1} have been obtained. The high-temperature values may be compared with the magnetic moment $\mu_{eff} = 3.62\ \mu_B$ at 286 K where the intermediate-spin (i.e. $S = {}^3/_2$) fraction may be estimated as $n_I \simeq 0.84$; the low temperature values may be set against the moment value $\mu_{eff} = 2.66\ \mu_B$ at 4.2 K where $n_I \simeq 0.34$. It should be noted that the [Fe(TMC)NO]$(BF_4)_2$ complex has a nearly linear FeNO group, a high NO stretching frequency of 1840 cm^{-1}, and a geometry intermediate between a square pyramid and a trigonal bipyramid.[18] On the other hand, the [Fe(salen)NO] complex, which shows a $S = {}^3/_2 - {}^1/_2$ transition of the discontinuous type, is characterized by Mössbauer parameters much more similar to those found for [Fe(salphen)NO], although the relaxation between the spin states is slow. Thus for the $S = {}^3/_2$ state, $\Delta E_Q = 0.352$ and $\delta^{IS} = +0.440$ mm s^{-1}, whereas for the $S = {}^1/_2$ state, $\Delta E_Q = 1.950$ and $\delta^{IS} = +0.281$ mm s^{-1} have been reported.[2] In [Fe(salen)NO], the FeNO group is strongly bent,[3] the NO stretching frequency is low[1] at 1712 cm^{-1}, and the coordination unit is not noticeably distorted toward trigonal-bipyramidal geometry. It may be therefore assumed that the most significant structural characteristics in [Fe(salphen)NO] are similar to those of [Fe(salen)NO] rather than to those observed for [Fe(TMC)NO]$(BF_4)_2$. The rapid relaxation between the spin states $S = {}^3/_2$ and $S = {}^1/_2$ in the [Fe(TMC)NO]$(BF_4)_2$ complex is therefore not a consequence of different coordination geometry of this complex and must be rather determined by other factors.

Acknowledgment. The authors appreciate financial support by the Deutsche Forschungsgemeinschaft, Bonn, West Germany.

Registry No. [Fe(salphen)NO], 73288-79-6.

(14) Federer, W. D.; Hendrickson, D. N. *Inorg. Chem.* **1984**, *23*, 3861.
(15) Federer, W. D.; Hendrickson, D. N. *Inorg. Chem.* **1984**, *23*, 3870.
(16) Ohshio, H.; Maeda, Y.; Takashima, Y. *Inorg. Chem.* **1983**, *22*, 2684.
(17) Maeda, Y.; Tsutsumi, N.; Takashima, Y. *Inorg. Chem.* **1983**, *23*, 2440.
(18) Hodges, K. D.; Wollmann, R. G.; Kessel, S. L.; Hendrickson, D. N.; Van Derveer, D. G.; Barefield, E. K. *J. Am. Chem. Soc.* **1979**, *101*, 906.

Contribution from the Department of Chemistry, University of Leuven, B-3030 Leuven, Belgium

Orbital Description of the Emitting Doublet States in Quadrate and Trigonal Chromium(III) Complexes

A. Ceulemans,* N. Bongaerts, and L. G. Vanquickenborne

Received October 10, 1986

The paper presents a simple orbital description of the emitting doublet states in hexacoordinated chromium(III) amine complexes of effective quadrate or trigonal symmetry. The principal parameter in this description is the energy splitting of the three t_{2g}-type d orbitals under the tetragonal or trigonal component of the ligand field. It is shown how this splitting affects the energies and wave functions of the lowest excited doublet states, from which emission occurs. The orbital characteristics of these wave functions are analyzed in terms of orbital occupation numbers. These numbers provide a simple orbital rationale for various excited-state properties, such as charge density distribution, metal–ligand bonding energies, Jahn–Teller instability, and solvent influence. The analysis attempts to clarify the phenomenological differences between the emission spectra of so-called ^2E and ^2T emitters of tetragonal symmetry. It also offers specific predictions with regard to the nature of the emitting states in trigonal complexes, such as $Cr(acac)_3$ and $Cr(bpy)_3^{3+}$.

I. Introduction

Recently Forster and co-workers[1] examined the emission spectra of over 40 quadrate mono- and disubstituted chromium(III) amine complexes in glassy solutions at 77 K. All these complexes were found to emit from their lowest doublet excited state. Depending on the octahedral parentage of the luminescent state, two quite different types of emission spectra were observed. So-called *^2E emitters*, i.e. complexes emitting from levels that are derived from the octahedral ^2E_g state, produce sharp emission spectra in the 650–710-nm region. On the other hand, *^2T emitters*, i.e. complexes that emit from doublet components of octahedral $^2T_{1g}$ parentage, are characterized by broad spectra, usually shifted to longer wavelengths.

It has also been found that at 77 K the nonradiative relaxation rates of the ^2E emitters are confined to a narrow range, $(0.9–3.5) \times 10^4$ s^{-1}, while a greater variation in decay rate prevails when the emission is due to a component of $^2T_{1g}$ origin.[2]

Finally, these two classes of emitters also display different solvent effects.[3] ^2E emitting states are only slightly affected by the solvent, whereas ^2T emission shifts to shorter wavelengths in hydroxylic solvents.

As it appears, ligand field calculations based on parameters that are extracted from the quartet region of the optical spectrum score reasonably well in predicting the nature of the emitting doublet state. Considerably less clarity is available as to the reasons the two types of emitters show such pronounced differences in spectral width, Stokes shift, lifetime, and solvent influence.

In an early paper, Hoggard and Schmidtke[4] have pointed to configurational differences between both emitting levels, without however providing a detailed description of these differences. As we have shown before,[5] such a description is not a trivial matter

(1) Forster, L. S.; Rund, J. V.; Fucaloro, A. F. *J. Phys. Chem.* **1984**, *88*, 5012. See also: Kirk, A. D.; Porter, G. B. *J. Phys. Chem.* **1980**, *84*, 887.
(2) Forster, L. S.; Rund, J. V.; Fucaloro, A. F.; Lin, S. H. *J. Phys. Chem.* **1984**, *88*, 5017.
(3) Fucaloro, A. F.; Forster, L. S.; Glover, S. G.; Kirk, A. D. *Inorg. Chem.* **1985**, *24*, 4242.
(4) Schmidtke, H.-H.; Hoggard, P. E. *Chem. Phys. Lett.* **1973**, *20*, 119.
(5) Ceulemans, A.; Beyens, D.; Vanquickenborne, L. G. *J. Am. Chem. Soc.* **1982**, *104*, 2988.

0020-1669/87/1326-1566$01.50/0

Table I. Tetragonal $M_S = {}^1/_2$ Components of the t_{2g}^3 Doublet Functions[a]

^2E_g State

$|^2A_{1g}\rangle = (1/2^{1/2})[|yz\ \overline{xz}\ xy| - |\overline{yz}\ xz\ xy|] = |^2E_g\ (1/2)\theta\rangle$

$|^2B_{1g}\rangle = (1/6^{1/2})[2|yz\ xz\ \overline{xy}| - |yz\ \overline{xz}\ xy| - |\overline{yz}\ xz\ xy|] = |^2E_g\ (1/2)\epsilon\rangle$

$^2T_{1g}$ State

$|^2A_{2g}\rangle = (1/2^{1/2})[|yz\ \overline{yz}\ xy| - |xz\ \overline{xz}\ xy|] = |^2T_{1g}\ (1/2)z\rangle$

$|^2E_g x\rangle = (1/2^{1/2})[|yz\ xz\ \overline{xz}| - |yz\ xy\ \overline{xy}|] = |^2T_{1g}\ (1/2)x\rangle$

$|^2E_g y\rangle = (1/2^{1/2})[|xz\ xy\ \overline{xy}| - |yz\ \overline{yz}\ xz|] = |^2T_{1g}\ (1/2)y\rangle$

$^2T_{2g}$ State

$|^2B_{2g}\rangle = (1/2^{1/2})[|yz\ \overline{yz}\ xy| + |xz\ \overline{xz}\ xy|] = |^2T_{2g}\ (1/2)\zeta\rangle$

$|^2E_g x\rangle = (1/2^{1/2})[|yz\ xy\ \overline{xy}| + |yz\ xz\ \overline{xz}|] = |^2T_{2g}\ (1/2)\xi\rangle$

$|^2E_g y\rangle = -(1/2^{1/2})[|xz\ xy\ \overline{xy}| + |yz\ \overline{yz}\ xz|] = -|^2T_{2g}\ (1/2)\eta\rangle$

[a] Each component is related to the octahedral t_{2g}^3 functions, published by Griffith.[11] Notice the minus sign in front of $|^2T_{2g}\ (1/2)\eta\rangle$. This sign reflects the tetragonal symmetry adaptation of the η component.

in view of the half-filled-shell nature of the parent octahedral doublet states. Proper wave functions, which incorporate the specific complementarity constraints for such half-filled-shell states, are available in the literature,[6,7] but what is currently lacking is a simple orbital analysis, capable of relating these wave functions to Forster's results.

In this perspective the aim of the present paper is to analyze the wave functions of the emitting states in quadrate chromium(III) amines in terms of simple orbital occupation numbers and to relate these numbers to the phenomenological differences between ^2E and ^2T emitters.

Furthermore, this analysis will be extended to the class of trigonally distorted hexacoordinated Cr(III) complexes, such as $Cr(acac)_3$ and $Cr(bpy)_3^{3+}$ (acac$^-$ = acetylacetonate, bpy = 2,2′-bipyridyl), by using our recently developed ligand field model[8] for complexes containing π-conjugated bidentate ligands. The emission properties of such trigonal complexes have not yet been studied in a systematic way.

II. Doublet Emission in Tetragonal d^3 Complexes

The considerations in this section pertain to the so-called quadrate chromium(III) amine complexes, CrN_5X, *trans*-CrN_4XY, and *cis*-CrN_4X_2, where X and Y are acido ligands such as H_2O, OH^-, F^-, and Cl^- and the N-coordination is due to NH_3, ethylenediamine, and pyridine. All these complexes have two identical coordination axes and therefore exhibit effective D_{4h} symmetry. Throughout, the ligators will be placed on the Cartesian axes and the z axis will be chosen to coincide with the effective fourfold axis. In the following we will treat successively the tetragonal t_{2g} orbitals, the energies and wave functions of the emitting levels, the corresponding orbital occupation numbers, and, finally, the resulting excited-state bonding scheme and its relevance to the observed emission.

IIa. Tetragonal t_{2g} Orbitals. In all quadrate chromium(III) amines the emitting doublet states are based on the octahedral t_{2g}^3 open-shell configuration, comprising the familiar d orbital set: xy, xz, and yz. In D_{4h} these t_{2g} orbitals transform as $b_{2g}(xy)$ and $e_g(xz,yz)$. According to the angular overlap model[9,10] (AOM) the associated orbital energies are given by

$$\epsilon(xy) = 4\bar{\pi}_{eq} \qquad \epsilon(xz,yz) = 2\bar{\pi}_{eq} + 2\bar{\pi}_{ax} \tag{1}$$

where $\bar{\pi}_{eq}$ refers to the average π parameter of the equatorial ligands on the x and y axes, while $\bar{\pi}_{ax}$ represents the average π parameter of the ligands on the z axis. The tetragonal splitting of the t_{2g} shell, denoted Δt_2, thus amounts to twice the difference between axial and equatorial π interactions:

$$\Delta t_2 = \epsilon(xz,yz) - \epsilon(xy) = 2(\bar{\pi}_{ax} - \bar{\pi}_{eq}) \tag{2}$$

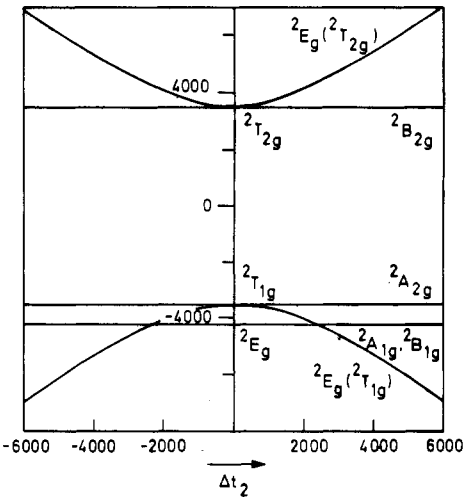

Figure 1. Energies of the t_{2g}^3 doublet states as a function of the tetragonal orbital splitting Δt_2, defined in eq 2. The center of the figure ($\Delta t_2 = 0$) represents the three parent octahedral states: ^2E_g, $^2T_{1g}$, and $^2T_{2g}$. Other symmetry labels refer to D_{4h} representations. Energy separations between the O_h levels were assumed to be 700 cm^{-1} for the $^2E_g \leftrightarrow {}^2T_{1g}$ distance and 7000 cm^{-1} for the $^2T_{1g} \leftrightarrow {}^2T_{2g}$ distance (cf. Appendix). Note that only the $^2E_g(D_{4h})$ components of $^2T_{1g}$ and $^2T_{2g}$ are affected by the tetragonal field (cf. eq 3). On the lowest energy curve a crossing point between levels of ^2E_g and $^2T_{1g}$ parentage is observed at $|\Delta t_2| \approx 2000$ cm^{-1}.

IIb. Energies and Wave Functions of the Emitting Levels. At the d^3 state level the octahedral t_{2g}^3 configuration gives rise to a $^4A_{2g}$ ground state and three excited doublet states, ordered as $^2E_g < {}^2T_{1g} < {}^2T_{2g}$. In D_{4h} these doublet states yield $^2A_{1g}$, $^2A_{2g}$, $^2B_{1g}$, $^2B_{2g}$, and two ^2E_g components. The corresponding tetragonal functions are listed in Table I. These functions were derived from the published octahedral t_{2g}^3 functions by using the appropriate $O_h \rightarrow D_{4h}$ subduction relations.[11] These subduction relations guarantee a strict symmetry standardization of the subrepresentation labels x and y. The advantage of using fixed x,y partners in Table I is that these x and y component labels will operate as genuine subquantum numbers and generate additional selection rules. As an example all interaction matrix elements between Ex and Ey functions are zero. Moreover the allowed matrix elements will be independent of the component label, a property that will be illustrated later on in eq 3.

Figure 1 shows the variation of the doublet energies as a function of increasing tetragonal perturbation. As the figure illustrates, the only energetic effect of the tetragonal field is a second-order interaction between the equisymmetric $^2E_g(D_{4h})$ states of $^2T_{1g}$ and $^2T_{2g}$ parentage. No first-order splittings of the octahedral levels are observed. Such splittings are indeed ruled out by the specific properties of half-filled-shell states.[5]

As a result ^2E emitters will be found in O_h and at low tetragonal fields where the quasi-degenerate $^2A_{1g}$ and $^2B_{1g}$ components of $^2E_g(O_h)$ parentage are below the $^2T_{1g}$ levels. At higher fields luminescence will switch over to ^2T parentage as the degenerate $^2E_g(D_{4h})$ component of $^2T_{1g}$ origin drops below the $^2A_{1g}$ and $^2B_{1g}$ levels. For the parameter values used in the example of Figure 1, the transition point between ^2E and ^2T emission is found at $|\Delta t_2| \approx 2000$ cm^{-1}.

Since the $^2A_{1g}$ and $^2B_{1g}$ components are not affected by the tetragonal splitting, the corresponding starting functions in Table I will remain valid wave forms for the ^2E emitting states

(6) Perumareddi, J. R. *J. Phys. Chem.* **1967**, *71*, 3144.
(7) Hoggard, P. E. *Z. Naturforsch., A: Phys., Phys. Chem., Kosmophys.* **1981**, *36A*, 1276.
(8) Ceulemans, A.; Den Dooven, M.; Vanquickenborne, L. G. *Inorg. Chem.* **1985**, *24*, 1153.
(9) Schäffer, C. E. *XIIth International Conference on Coordination Chemistry, Sydney 1969*; Butterworths: London, 1970; p 361.
(10) Vanquickenborne, L. G.; Ceulemans, A. *J. Am. Chem. Soc.* **1977**, *99*, 2208.
(11) Griffith, J. S. *The Theory of Transition-Metal Ions*; Cambridge University Press: Cambridge, England, 1971.

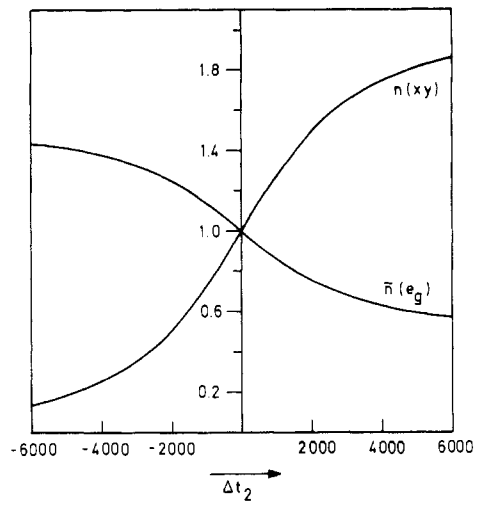

Figure 2. Orbital occupation numbers for the tetragonal Φ_x and Φ_y components as a function of the tetragonal splitting. $n(xy)$ represents the population of the xy orbital; $\bar{n}(e_g)$ is the average occupation number of the xz and yz orbitals of e_g symmetry (cf. eq 8a–c). In O_h both $n(xy)$ and $\bar{n}(e_g)$ are equal to 1. A positive tetragonal splitting will lower the energy of the xy orbital relative to the energy of xz and yz orbitals and give rise to an increase of $n(xy)$ and a decrease of $\bar{n}(e_g)$. For a negative tetragonal splitting the opposite charge flow is observed. Hence, in either case one has a preferential occupation of the lower lying orbitals and a simultaneous depopulation of the higher lying ones.

throughout the entire quadrate chromium amine series. On the other hand, wave functions for the ^2T emitting states will explicitly depend on the tetragonal splitting and must be obtained from a diagonalization of a 2×2 interaction matrix, which describes the mixing between the two degenerate components of $^2T_{1g}$ and $^2T_{2g}$ parentage. As indicated before, this matrix is identical for x and y components:

$$\begin{array}{lcc} & |^2E_g(^2T_{1g})i\rangle & |^2E_g(^2T_{2g})i\rangle \\ \langle^2E_g(^2T_{1g})i| & -D/2 & \Delta t_2 \\ \langle^2E_g(^2T_{2g})i| & \Delta t_2 & D/2 \end{array} \qquad (3)$$

$$i = x \text{ or } y$$

In this matrix the off-diagonal element, Δt_2, simply corresponds to the tetragonal orbital splitting, defined in eq 2. The parameter D represents the $^2T_{1g}$–$^2T_{2g}$ energy gap in the parent octahedral complex. For $Cr(NH_3)_6^{3+}$, D is on the order[12] of 7000 cm^{-1}. This is somewhat less than the value one would obtain in the strong-field limit, which is given by $6B + 2C$ in the Racah parametrization. The observed reduction is due to configuration interaction with higher excited $t_{2g}^2e_g$ states, mainly affecting the upper $^2T_{2g}$ level.

The roots of the matrix in eq 3, relative to the configuration average of the $^2T_{1g}$ and $^2T_{2g}$ states, are given by

$$\epsilon_\pm = \pm[D^2/4 + (\Delta t_2)^2]^{1/2} \qquad (4)$$

Eigenfunctions that are associated with the lower root, ϵ_-, will be represented as $|\Phi_x\rangle$ and $|\Phi_y\rangle$ and obey the expressions

$$|\Phi_x\rangle = (1 + \alpha^2)^{-1/2}[|^2E_g(^2T_{1g})x\rangle - \alpha|^2E_g(^2T_{2g})x\rangle]$$

$$|\Phi_y\rangle = (1 + \alpha^2)^{-1/2}[|^2E_g(^2T_{1g})y\rangle - \alpha|^2E_g(^2T_{2g})y\rangle] \qquad (5)$$

The mixing coefficient α has the value

$$\alpha = \frac{\Delta t_2}{D/2 + [D^2/4 + (\Delta t_2)^2]^{1/2}} \qquad (6)$$

Similar expressions have been obtained before by Zink,[13] although his results should be corrected for a phase inconsistency in the definition of the y component. Furthermore, in ref 13 the mixing coefficient was allowed to vary over a wide range from −10 to +10. This conflicts with eq 6, where it is shown that the minimal value of α cannot be lower than −1 for $\Delta t_2 \rightarrow -\infty$ and the maximal value cannot exceed +1 for $\Delta t_2 \rightarrow +\infty$.

It is true that configuration interaction with $t_{2g}^2e_g$ states[6] and spin–orbit coupling interactions[7] still may give rise to further refinements of the wave functions derived here. However, more complete calculations by Flint and Matthews have demonstrated that—at least for the Cr(III) ions—such effects are of minor significance.[14] Moreover, to the extent that they are operative, they do not introduce further configurational differences between both classes of emitters. For these reasons, the subsequent orbital analysis of Forster's results can safely be based on the $^2A_{1g}$ and $^2B_{1g}$ functions listed in Table I for ^2E emitters, and on the Φ_x and Φ_y components, specified in eq 5, for the ^2T emitters.

IIc. Orbital Occupation Numbers. A precise idea of the configurational differences between the four wave functions, obtained in the previous paragraph, and the resulting charge density distributions can most easily be gathered from a straightforward orbital population analysis. For multideterminantal functions, such as our candidate emitting states, the occupation number of a particular tetragonal symmetry orbital corresponds to the sum of the orbital occupation numbers in the single-determinantal terms, weighted by the squares of the associated expansion coefficients. The results of such an analysis for the different emitting states are

(i) ^2E emitting states

$$^2A_{1g}: \; n(xy) = n(xz) = n(yz) = 1 \qquad (7a)$$

$$^2B_{1g}: \; n(xy) = n(xz) = n(yz) = 1 \qquad (7b)$$

(ii) ^2T emitting states

$$\Phi_x: \; n(xy) = 1 + 2\alpha/(1 + \alpha^2); \; n(xz) = 1 - 2\alpha/(1 + \alpha^2); \; n(yz) = 1 \qquad (8a)$$

$$\Phi_y: \; n(xy) = 1 + 2\alpha/(1 + \alpha^2); \; n(xz) = 1; \; n(yz) = 1 - 2\alpha/(1 + \alpha^2) \qquad (8b)$$

Note that for both Φ functions the average occupation number of the e_g orbitals, $\bar{n}(e_g)$, has the same value, as indicated in eq 8c:

$$\Phi_x \text{ or } \Phi_y: \; \bar{n}(e_g) = \tfrac{1}{2}[n(xz) + n(yz)] = 1 - \alpha/(1 + \alpha^2) \qquad (8c)$$

First of all, these equations illustrate that in O_h ($\alpha = 0$) all four component functions have one electron per t_{2g} orbital. As we have argued before,[5] such uniform charge distribution is a typical characteristic of half-filled-shell states. Since the ^2E emitting levels are not modified by the tetragonal field, they will preserve this octahedral distribution in the substituted amine complexes. On the other hand, for the ^2T levels, departure from octahedral symmetry will cause a gradual polarization of the charge distribution between the axial and equatorial sites of the complex. This is further illustrated in Figure 2, where the average orbital occupation numbers for Φ_x and Φ_y are plotted as a function of the tetragonal orbital splitting.

This figure in conjunction with eq 2 and 8 shows that for a positive orbital splitting ($\epsilon(xz,yz) > \epsilon(xy)$) the tetragonal perturbation causes a gradual depletion of the higher lying xz and yz orbitals and a charge flow into the xy orbital. Conversely for negative Δt_2 values the xy orbital is depopulated, giving rise to a charge flow into the lower lying xz and yz orbitals. Hence, for either sign of the tetragonal splitting, the lower t_{2g} orbitals always show increased population while the higher ones become more vacant.

We remark that it requires quite strong tetragonal fields to empty a t_{2g} orbital to an appreciable extent. Even in very polarized

(12) Lever, A. B. P. *Inorganic Electronic Spectroscopy*, 2nd ed.; Elsevier: New York, 1984.
(13) Zink, J. I. *Inorg. Chem.* **1973**, *12*, 1957.
(14) Flint, C. D.; Matthews, A. P. *Inorg. Chem.* **1975**, *14*, 1008.

complexes this process is not carried to completion. As an example, with the parameters that are listed in the Appendix we may calculate the orbital occupation numbers in a strongly perturbed ^2T emitting complex, such as *trans*-$Cr(NH_3)_4F_2^+$. One has $\Delta t_2 = 3760\ cm^{-1}$ and $\alpha = 0.44$, yielding for the Φ states $n(xy) = 1.74$ and $\bar{n}(e_g) = 0.63$. In the next section we will confront these results with the reported ^2E and ^2T emitting properties.

IId. Bond Energies and Emission Behavior. Orbital occupation numbers not only provide a clear picture of the charge density distribution in the emitting states but also can be used to derive excited-state bond energies. These energies are of prime importance in the determination of the emission properties.

A simple model that relates orbital occupation numbers to individual M–L bond energies has been developed before[10,15] in a study of the leaving-ligand problem in d^3 and d^6 photochemistry. According to this model, the bond energy, I(M–L), for a π-donor-type ligand L is given by

$$I(\text{M–L}) = \sum_i [2 - n(d_i)]\langle d_i|V_L|d_i\rangle \qquad (9)$$

where the summation runs over the five d orbitals, $n(d_i)$ being the occupation number of the ith d orbital. The matrix element in V_L symbolizes the contribution of ligand L in the AOM energy of the ith orbital. As a result I(M–L) will be expressed in terms of the AOM parameters σ_L and π_L of the ligand concerned. The fact that such a partitioning in individual ligand contributions is possible is due to the ligand additivity property of the AOM potential.

For the quartet ground state, where all three t_{2g} orbitals are singly occupied and the two e_g orbitals are empty, the I(M–L) values simply correspond to[10]

$$I(\text{M–L}) = 2\sigma_L + 2\pi_L \qquad (10)$$

Exactly the same bond energies will be obtained for the A_{1g} and B_{1g} components of ^2E emitters, since these components have exactly the same orbital occupation as the ground level (cf. eq 7). This is in line with our earlier claim[5] that half-filled-shell states are largely imperturbable entities, which resist configurational changes. Accordingly, the equilibrium geometries of these excited states will coincide with the ground-state equilibrium geometry, and a sharp-line luminescence spectrum is expected. This is indeed a typical characteristic of ^2E emitters.[1]

In contrast, the bond energies of the ^2T emitting states require different expressions, which will be denoted by I^*(M–L) and may be obtained from the general formula by inserting the average occupational numbers for Φ_x and Φ_y, previously given in eq 8. The appropriate I^* quantities for a *trans*-CrN_4X_2 complex are

$$I^*(\text{Cr–X}) = 2\sigma_X + \left[2 + \frac{2\alpha}{1+\alpha^2}\right]\pi_X$$
$$I^*(\text{Cr–N}) = 2\sigma_N + \left[2 - \frac{\alpha}{1+\alpha^2}\right]\pi_N \qquad (11)$$

If X is a π-donor ligand as compared to N, the tetragonal orbital splitting Δt_2 and the mixing coefficient α will be positive. As a result Cr–X bonds will be strengthened by an amount $2\pi_X\alpha/(1+\alpha^2)$ as compared to the ground-state values in eq 10. On the other hand, the equatorial bonds will be weakened to a smaller extent. Especially the increase of Cr–X bond energies can lead to sizable changes in bond lengths. As an example, for *trans*-$Cr(py)_2F_2^+$ the estimated[14] shortening of the Cr–F distance in the ^2T emitting level amounts to about 0.1 Å. Such changes in geometry may give rise to the appearance of Franck–Condon progressions and appreciable Stokes shifts, in accordance with the reported emission behavior of ^2T emitters.[1,14,16,17]

As a further illustration of the I^* methodology we also present I^* values for the Φ functions in *cis*-CrN_4X_2, where again X is a π donor relative to N. One has

$$I^*(\text{Cr–X}) = 2\sigma_X + \left[2 - \frac{\alpha}{1+\alpha^2}\right]\pi_X$$
$$I^*(\text{Cr–N}_{eq}) = 2\sigma_N + \left[2 - \frac{\alpha}{1+\alpha^2}\right]\pi_N \qquad (12)$$
$$I^*(\text{Cr–N}_{ax}) = 2\sigma_N + \left[2 + \frac{2\alpha}{1+\alpha^2}\right]\pi_N$$

For cis complexes AOM predicts (cf. eq 2) a negative orbital splitting Δt_2, which in addition will only be half as large as in the corresponding trans complexes. In consequence the mixing coefficient α will be negative but configuration mixing will be less pronounced than for the trans complexes. Therefore, the Cr–X bond is again predicted to be strengthened, though not to the same extent as for the trans isomer. As an example, using the parameters that are collected in the Appendix, one calculates the following for *cis*-$Cr(NH_3)_4F_2^+$: $\alpha = -0.25$, $I^*(\text{Cr–F}) = 2\sigma_F + 2.24\pi_F$. These values are substantially lower than the values for *trans*-$Cr(NH_3)_4F_2^+$: $\alpha = 0.44$, $I^*(\text{Cr–F}) = 2\sigma_F + 2.74\pi_F$.

Most of the cis complexes that have been examined to date seem to be ^2E emitters,[1,18] which is not too surprising in view of their reduced tetragonal splitting as compared to that of the trans complexes. Special cases are the *cis*-dihydroxo complexes *cis*-$Cr(NH_3)_4(OH)_2^+$ and *cis*-$Cr(en)_2(OH)_2^+$. In alcohol–water glasses these complexes behave like ^2E emitters, whereas in DMF–water glasses they show the spectral characteristics of ^2T emitters.[3] Apparently in the diagram in Figure 1 these complexes are close to the ^2E–^2T transition point, where a slight change in solvent influence is sufficient to change emission characteristics. Interestingly in the DMF–water glass the Stokes shift is considerably less than for the corresponding *trans*-dihydroxo complexes, in agreement with the predictions from eq 12.

In addition to these bonding considerations and the concomitant bond length changes, attention should be drawn to two other effects of $^2T_{1g}$–$^2T_{2g}$ configurational mixing, which will also influence the emission properties. First of all, one must take into account possible Jahn–Teller activity of the emitting states. As we have demonstrated before, the octahedral levels are free from Jahn–Teller activity as a result of the half-filled-shell selection rules.[5,19] The same rules prevent vibronic coupling between the quasi-degenerate $^2A_{1g}$ and $^2B_{1g}$ components of ^2E emitters. However, these rules are no longer valid for the x and y components of quadrate ^2T emitters, since configurational mixing destroys the isotropic charge distribution in these states. This may be observed in eq 8a,b, which show that for $\alpha \neq 0$, Φ_x and Φ_y no longer share the same occupational numbers for the degenerate xz and yz orbitals. As a result the $^2E_g(D_{4h})$ state of a ^2T emitter will acquire Jahn–Teller instability. It is well-known that the resulting instability can give rise to additional vibronic band structure and thus may contribute to the spectral broadening of ^2T emission bands.

Finally it should also be remarked that the charge redistribution in the excited state of ^2T emitters may induce solvational changes. More specifically, solvent interactions may be enhanced in those interligand regions where charge density is diminished and the metal ion becomes more exposed to the environment. Such effects must certainly be envisaged in the glassy solutions studied by the groups of Forster and Kirk.[3]

III. Extension to Trigonal d^3 Complexes

This section will be concerned with an extension of the foregoing orbital analysis to the important class of trigonally distorted hexacoordinated d^3 complexes. Special attention will be focused

(15) Vanquickenborne, L. G.; Ceulemans, A. *Coord. Chem. Rev.* **1983**, *48*, 157.
(16) Flint, C. D.; Matthews, A. P. *J. Chem. Soc., Faraday Trans. 2* **1974**, *70*, 1307.
(17) Decurtins, S.; Güdel, H. U.; Neuenschwander, K. *Inorg. Chem.* **1977**, *16*, 796.
(18) Flint, C. D.; Matthews, A. M.; O'Grady, P. J. *J. Chem. Soc., Faraday Trans. 2* **1977**, *73*, 655.
(19) For a rigorous proof of Jahn–Teller inactivity of half-filled-shell states, see: Ceulemans, A. *Meded. K. Acad. Wet., Lett. Schone Kunsten Belg., Kl. Wet.* **1985**, *46*, 82.

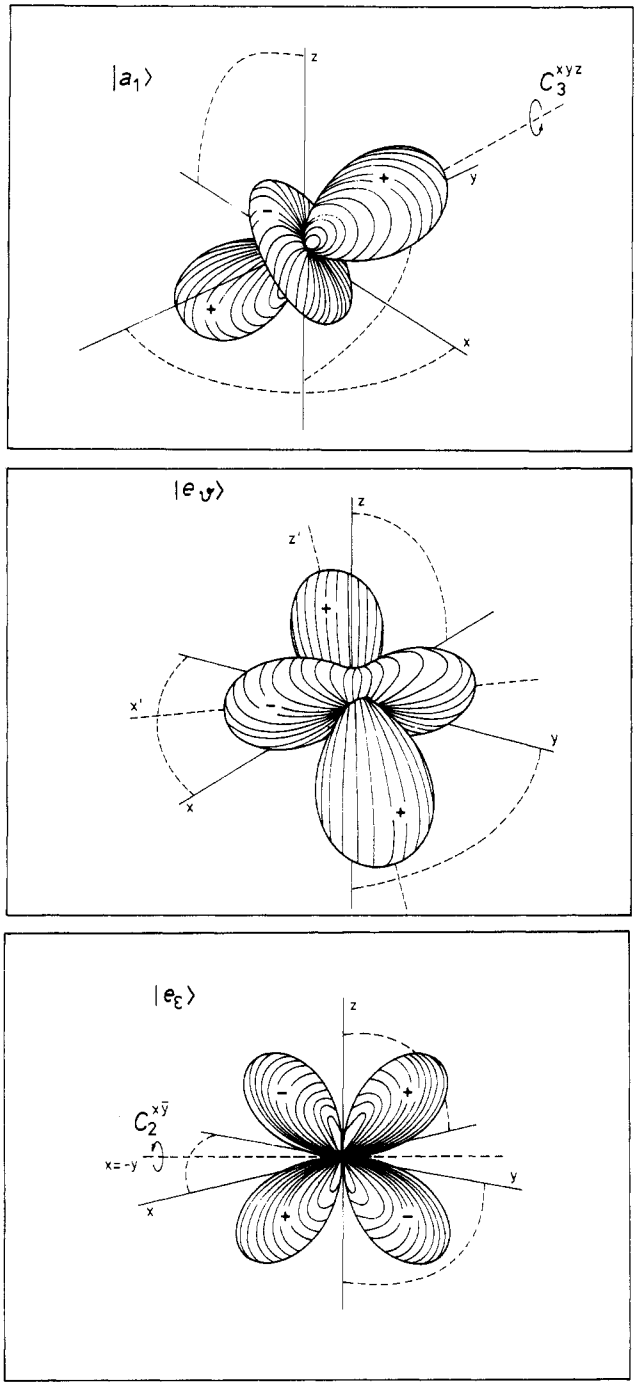

Figure 3. Shapes of the three trigonal t_{2g} orbitals a_1, e_θ, and e_ϵ (cf. eq 13) and their orientations in a trischelated structure. Ligator atoms are positioned on the Cartesian axes. The direction of the C_3^{xyz} symmetry axis is also indicated. The shapes of these orbitals are discussed in the text (section IIIa).

on the emission properties of trischelated complexes containing unsaturated bidentate ligands, such as 2,2'-bipyridyl (bpy) or acetylacetonate ($acac^-$). Already in 1961 Orgel[20] indicated that such complexes may exhibit a pronounced trigonal splitting of the t_{2g} orbitals, as a result of electronic interactions with the conjugated bridges.

For simplicity the complexes involved will be assumed to be strictly orthoaxial, with the six ligator atoms on the Cartesian axes, the chelate bridges forming a Λ- or Δ-type helix around the trigonal axis C_3^{xyz} (cf. Figure 3). The actual symmetry of such complexes is D_3, but the d orbitals may be classified under an effective D_{3d} symmetry. The subsequent section will be organized

(20) Orgel, L. E. *J. Chem. Soc.* **1961**, 3683.

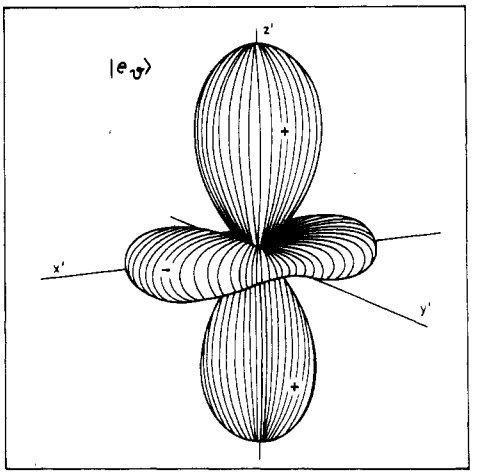

Figure 4. Drawing of the unusual e_θ orbital in an upright position. The primed coordinate axes are defined in the text (cf. eq 15). Note the ellipsoidal orbital form in the equatorial plane.

in the same way as section II, while particular attention will be devoted to the representation of the real t_{2g} orbitals in a trigonal basis.

IIIa. Trigonal t_{2g} Orbitals. Under the operations of D_3 the t_{2g} orbitals transform as a_1 and e. In the Cartesian frame of Figure 3 these orbitals may be obtained from the tetragonal ones by the transformation

$$\begin{aligned} |a_1\rangle &= (1/3^{1/2})(|xy\rangle + |yz\rangle + |xz\rangle) \\ |e_\theta\rangle &= (1/6^{1/2})(2|xy\rangle - |yz\rangle - |xz\rangle) \\ |e_\epsilon\rangle &= (1/2^{1/2})(|yz\rangle - |xz\rangle) \end{aligned} \tag{13}$$

The θ and ϵ labels thereby denote canonical components, which strictly obey the symmetry relations

$$\begin{aligned} C_3^{xyz}|e_\theta\rangle &= -(1/2)|e_\theta\rangle + (3^{1/2}/2)|e_\epsilon\rangle \\ C_3^{xyz}|e_\epsilon\rangle &= -(3^{1/2}/2)|e_\theta\rangle - (1/2)|e_\epsilon\rangle \\ C_2^{xy}|e_\theta\rangle &= |e_\theta\rangle \\ C_2^{xy}|e_\epsilon\rangle &= -|e_\epsilon\rangle \end{aligned} \tag{14}$$

Here C_3^{xyz} is the trigonal symmetry axis of the trischelated structure. C_2^{xy} is the twofold axis in the xy plane at the $x = -y$ direction. As usual these symmetry operations leave the Cartesian axes immobile but rotate orbital functions in a counterclockwise sense. Figure 3 offers perspective drawings of the forms and orientations of these trigonal t_{2g} orbitals in the trischelated structure. As can be seen from the figure the a_1 orbital corresponds to a d_{z^2}-shaped orbital, with its direction of major amplitude pointing along the threefold axis. The e_ϵ orbital has the shape of the usual tetragonal t_{2g} orbitals. Its nodal planes are the horizontal $z = 0$ plane and the diagonal $x = y$ plane. In contrast e_θ is seen to have an unusual shape, which may most easily be described in the primed coordinate system of Figure 3. In this system the x' axis corresponds to the direction of the C_2^{xy} axis. The z' axis is defined by the aximuthal coordinates $\theta = \pi/2 - \tau/4$ and $\varphi = 5\pi/4$, where τ is the tetrahedral angle of 109.46°. From the AOM rotation technique the e_θ orbital can be expressed in the primed system as

$$|e_\theta\rangle = \frac{1 + 3^{1/2}}{8^{1/2}}|z'^2\rangle + \frac{1 - 3^{1/2}}{8^{1/2}}|x'^2 - y'^2\rangle \tag{15}$$

$|z'^2\rangle$ and $|x'^2 - y'^2\rangle$ symbolizing the usual d_{z^2} and $d_{x^2-y^2}$ functions in the primed coordinate system. In Figure 4 the e_θ drawing has been resumed with z' in an upright position. From this figure and eq 15 it is clear that e_θ may best be visualized as a distorted d_{z^2} function with an ellipsoidal torus instead of the usual cylindrical equator. Despite their different shapes it must be kept in mind that the e_θ and e_ϵ orbitals belong to the same e representation and thus are strictly degenerate.

Table II. Trigonal $M_S = {}^1/_2$ Components of the t_{2g}^3 Doublet Functions[a]

^2E_g State

$$|^2E\theta\rangle = (1/6^{1/2})[2^{1/2}|a_1\ \bar{a}_1\ \theta| - 2^{1/2}|\theta\ \epsilon\ \bar{\epsilon}| + |a_1\ \theta\ \bar{\theta}| - |a_1\ \epsilon\ \bar{\epsilon}|] = |^2E_g\ (1/2)\theta\rangle$$
$$|^2E\epsilon\rangle = (1/6^{1/2})[2^{1/2}|a_1\ \bar{a}_1\ \epsilon| - 2^{1/2}|\theta\ \bar{\theta}\ \epsilon| + |a_1\ \bar{\theta}\ \epsilon| - |a_1\ \theta\ \bar{\epsilon}|] = |^2E_g\ (1/2)\epsilon\rangle$$

$^2T_{1g}$ State

$$|^2A_2\rangle = (1/6^{1/2})[2|\bar{a}_1\ \theta\ \epsilon| - |a_1\ \bar{\theta}\ \epsilon| + |a_1\ \theta\ \bar{\epsilon}|] = (1/3^{1/2})[|^2T_{1g}\ (1/2)x\rangle + |^2T_{1g}\ (1/2)y\rangle + |^2T_{1g}\ (1/2)z\rangle]$$
$$|^2E\theta\rangle = (1/6^{1/2})[-2^{1/2}|a_1\ \theta\ \bar{\theta}| + 2^{1/2}|a_1\ \epsilon\ \bar{\epsilon}| - |\theta\ \epsilon\ \bar{\epsilon}| + |a_1\ \bar{a}_1\ \theta|] = (1/2^{1/2})[|^2T_{1g}\ (1/2)x\rangle - |^2T_{1g}\ (1/2)y\rangle]$$
$$|^2E\epsilon\rangle = (1/6^{1/2})[2^{1/2}|a_1\ \theta\ \bar{\epsilon}| - 2^{1/2}|a_1\ \bar{\theta}\ \epsilon| + |a_1\ \bar{a}_1\ \epsilon| - |\theta\ \bar{\theta}\ \epsilon|] = (1/6^{1/2})[|^2T_{1g}\ (1/2)x\rangle + |^2T_{1g}\ (1/2)y\rangle - 2|^2T_{1g}\ (1/2)z\rangle]$$

$^2T_{2g}$ State

$$|^2A_1\rangle = (1/2^{1/2})[|a_1\ \epsilon\ \bar{\epsilon}| + |a_1\ \theta\ \bar{\theta}|] = (1/3^{1/2})[|^2T_{2g}\ (1/2)\xi\rangle + |^2T_{2g}\ (1/2)\eta\rangle + |^2T_{2g}\ (1/2)\zeta\rangle]$$
$$|^2E\theta\rangle = (1/2^{1/2})[|a_1\ \bar{a}_1\ \theta| + |\theta\ \epsilon\ \bar{\epsilon}|] = (1/6^{1/2})[2|^2T_{2g}\ (1/2)\zeta\rangle - |^2T_{2g}\ (1/2)\xi\rangle - |^2T_{2g}\ (1/2)\eta\rangle]$$
$$|^2E\epsilon\rangle = (1/2^{1/2})[|a_1\ \bar{a}_1\ \epsilon| + |\theta\ \bar{\theta}\ \epsilon|] = (1/2^{1/2})[|^2T_{2g}\ (1/2)\xi\rangle - |^2T_{2g}\ (1/2)\eta\rangle]$$

[a] The orbital basis consists of the real trigonal t_{2g} functions $|a_1\rangle$, $|e_\theta\rangle$, and $|e_\epsilon\rangle$, specified in eq 13. Each component is related to the octahedral t_{2g}^3 functions, published by Griffith.[11]

If one compares the angular distributions of the a_1 and e orbitals, as depicted in Figures 3 and 4, one is led to the conclusion that these orbitals extend over different sites of the trischelated complex: the a_1 orbital density is mainly concentrated on the open triangular faces of the octahedron while both e orbitals are more oriented toward the bridging atoms and the so-called interligand "pockets".

It should be remarked that under D_3 the octahedral e_g orbitals d_{z^2} and $d_{x^2-y^2}$ transform according to the irreducible e representation, so that orbital interactions between the e_g set and the e-type t_{2g} functions become symmetry-allowed. These interactions might induce further modifications of the $|e_\theta\rangle$ and $|e_\epsilon\rangle$ functions of eq 13.

As for the orbital energies, the most relevant quantity in the present discussion is the energy splitting of the t_{2g} orbitals by the trigonal field. This splitting will be defined analogously to the tetragonal splitting Δt_2 in the previous section, but it will be labeled $\Delta\tau_2$ to avoid confusion between both definitions. Hence we write

$$\Delta\tau_2 = \epsilon(e) - \epsilon(a_1) \tag{16}$$

In complexes where this splitting originates from trigonal distortions of the octahedral frame, the AOM formalism may be used to calculate its sign and magnitude from the distortion angles and the σ and π parameters of the ligating atoms. However, such static effects are often rather weak and we will be more interested in the pronounced electronic effects that arise in trischelated complexes containing unsaturated bidentate moieties. Orgel[20] has indeed pointed out that in these complexes the electronic interaction between the t_{2g} orbitals and the π-type molecular orbitals on the ligands may give rise to a strong trigonal splitting of the t_{2g} shell. Elsewhere[8] we have shown how this trigonal Orgel effect may be expressed in AOM-like π-parameters, which refer to the definite phase relationships between the pπ-type frontier orbitals at the ligating atoms on both ends of a π-conjugated chain. If in the frontier MO on the bidentate ligand the ligator pπ functions are in phase, a ψ-type Orgel effect results. As explained in ref 8, the trigonal splitting in this case is given by

$$\Delta\tau_2(\psi) = 3\ \pi_\perp(\psi) \tag{17a}$$

where we have explicitly added the ψ label to indicate the type of Orgel effect considered. In this equation $\pi_\perp$ represents the AOM interaction between the pπ ligator orbital, orthogonal to the bidentate plane, and the metal d orbitals, as defined in ref 8. On the other hand, if in the frontier MO of the ligand the pπ functions on the ligating atoms are out of phase, a χ-type coupling is involved and an inverse sign relation will be obtained:

$$\Delta\tau_2(\chi) = -3\ \pi_\perp(\chi) \tag{17b}$$

In ref 8 it is pointed out that in principle more than one MO interaction can be important so that both ψ and χ effects may be present. Hence, in the more general case the trigonal splitting is obtained as a result of both ψ and χ interactions:

$$\Delta\tau_2 = 3\pi_\perp(\psi) - 3\pi_\perp(\chi) \tag{17c}$$

Interestingly, if ψ interactions are of the donor type ($\pi_\perp(\psi) > 0$) while χ interactions are of the acceptor type ($\pi_\perp(\chi) < 0$)—or vice versa—their combined effect will give rise to a more pronounced trigonal splitting, due to the minus sign in eq 17c.

For simplicity we have assumed that the complex is nearly orthoaxial so that the aforementioned trigonal e_g–t_{2g} mixing is negligible and does not contribute to the t_{2g} splitting. A simple MO picture of the unsaturated ligands in conjunction with eq 17 may now be used to anticipate the sign of the trigonal splitting.[8] So for a five-membered chelate chain, such as in acac, one expects that the trigonal field will be dominated by a ligand donor level of the ψ type; this means that $\pi_\perp(\psi)$ will be large and positive, while $\pi_\perp(\chi)$ will be close to zero. Hence, in $Cr(acac)_3$ the trigonal splitting is predicted to be positive, with the e level above a_1. This is in line with experimental evidence.[21]

For a four-membered chelate chain, such as in bpy, the π interactions should primarily originate from a ψ-type acceptor level, so that $\pi_\perp(\psi)$ will be negative, with again $\pi_\perp(\chi) \approx 0$. As a result one anticipates for $Cr(bpy)_3^{3+}$ a negative orbital splitting with the a_1 level at higher energy than the e level. Unequivocal experimental confirmation of this predicted orbital ordering is still lacking.

IIIb. Energies and Wave Functions of the Emitting Levels. In D_3 the t_{2g}^3 states yield $^2A_1$, $^2A_2$, and three ^2E sublevels. Corresponding component functions can be obtained from the standard subduction methods, which have been tabulated by Griffith.[11] The resulting functions are listed in Table II. They have been expressed in the trigonal orbital basis of eq 13. As already mentioned, the subduction method guarantees a strict symmetry standardization of the subrepresentation labels θ and ϵ. Hence, all θ,ϵ partners in Table II exactly obey the symmetry relations in eq 14. In consequence interaction matrix elements between $E\theta$ and $E\epsilon$ functions will be zero, while the value of the non-zero matrix elements will be independent of the component label. Similar wave functions in a complex trigonal basis have been listed by Perumareddi.[6]

Figure 5 represents the variation of the doublet energies as a function of increasing trigonal perturbation. As the figure shows, there are no first-order splittings of the octahedral multiplets. The unique levels $^2A_1$ and $^2A_2$ remain totally invariant, while the three equisymmetric ^2E levels show only second-order variations, as a result of interstate interactions. The main difference between the present trigonal splitting scheme and the tetragonal correlation diagram in Figure 1 is that *in the trigonal case there is no crossing point on the lowest doublet curve*. All trigonal phosphors thus essentially belong to one and the same class! Since each state of the octahedral doublet manifold yields a ^2E component, all three parent doublets will contribute in the wave function for this class of emitters. As one moves across a series of trigonal complexes with increasing t_{2g} splitting, the composition of this wave function will gradually change, but sudden alterations, as in the ^2E–^2T transition point of the quadrate series, will be excluded.

A precise description of the lowest excited state in trigonal complexes requires the solution of a 3 × 3 matrix problem, which

(21) Piper, T. S.; Carlin, R. L. *J. Chem. Phys.* **1962**, *36*, 3330.

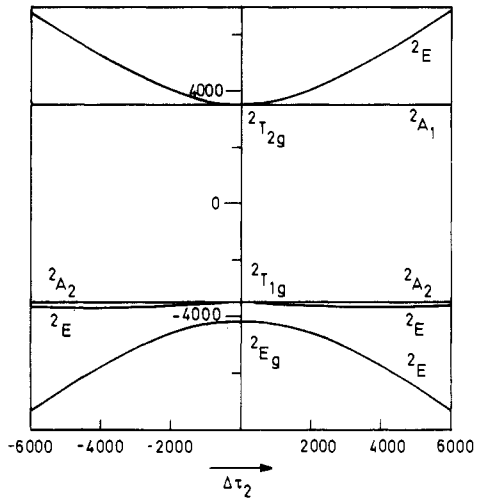

Figure 5. Energies of the t_{2g}^3 doublet states as a function of the trigonal orbital splitting $\Delta\tau_2$, defined in eq 16. In the center of the figure one recognizes the parent O_h states ^2E_g, $^2T_{1g}$, and $^2T_{2g}$. Other symmetry labels refer to D_3 representations. Only the three equisymmetric $^2E(D_3)$ components are affected by the trigonal field. In contrast to the tetragonal correlation diagram of Figure 1, in the present figure there is no crossing point on the lowest energy curve. Hence, all trigonal emitters are of $^2E_g(O_h)$ parentage.

represents the interaction of the three ^2E states (for θ and ϵ components). It is given by

	$\|^2E(^2E_g)i\rangle$	$\|^2E(^2T_{1g})i\rangle$	$\|^2E(^2T_{2g})i\rangle$	
$\langle^2E(^2E_g)i\|$	$-D/2 - D'$	0	$-(2^{1/2}/3^{1/2})\Delta\tau_2$	(18)
$\langle^2E(^2T_{1g})i\|$	0	$-D/2$	$-(1/3^{1/2})\Delta\tau_2$	
$\langle^2E(^2T_{2g})i\|$	$-(2^{1/2}/3^{1/2})\Delta\tau_2$	$-(1/3^{1/2})\Delta\tau_2$	$D/2$	

$i = \theta$ or ϵ

D represents the $^2T_{1g}$–$^2T_{2g}$ gap, $\Delta\tau_2$ is the trigonal splitting, defined earlier in eq 16, and D' is the energy gap between the parent $^2T_{1g}$ and ^2E_g states. This gap arises mainly through configuration interaction with higher excited doublet states and ranges from 500 cm^{-1} in strong-field complexes[22] such as $Cr(CN)_6^{3-}$ to over 1000 cm^{-1} in weak-field complexes[23] such as CrF_6^{3-}.

General solutions of the matrix problem are rather intractable, so that in practice the eigenvalues and wave functions can better be determined by numerical diagonalization, starting from known values for the parameters D, D', and $\Delta\tau_2$. Wave function solutions for the lowest energy emitting levels will be denoted as Ψ_θ and Ψ_ϵ. Interestingly simple analytic approximations of these wave functions may easily be found if the parameter D' is put equal to zero. The lowest eigenvalue and the associated eigenvectors in this approximation will be labeled by a superscript zero, respectively, as ϵ_-^0 and as Ψ_θ^0 and Ψ_ϵ^0. One has

$$\epsilon_-^0 = -[D^2/4 + (\Delta\tau_2)^2]^{1/2} \tag{19}$$

$$|\Psi_\theta^0\rangle = (1 + \beta^2)^{-1/2}[(2^{1/2}/3^{1/2})|^2E(^2E_g)\theta\rangle + (1/3^{1/2})|^2E(^2T_{1g})\theta\rangle + \beta|^2E(^2T_{2g})\theta\rangle]$$

$$|\Psi_\epsilon^0\rangle = (1 + \beta^2)^{-1/2}[(2^{1/2}/3^{1/2})|^2E(^2E_g)\epsilon\rangle + (1/3^{1/2})|^2E(^2T_{1g})\epsilon\rangle + \beta|^2E(^2T_{2g})\epsilon\rangle] \tag{20}$$

In this equation we introduce a trigonal mixing coefficient β, which follows exactly the same definition as its tetragonal counterpart α in eq 6. Hence

$$\beta = \frac{\Delta\tau_2}{D/2 + [D^2/4 + (\Delta\tau_2)^2]^{1/2}} \tag{21}$$

(22) Witzke, H. *Theor. Chim. Acta* **1971**, *20*, 171.
(23) Dubicki, L.; Ferguson, J.; van Oosterhout, B. *J. Phys. C.* **1980**, *13*, 2791.

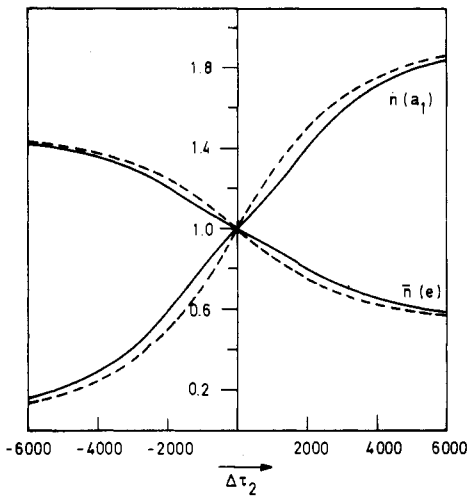

Figure 6. Orbital occupation for the lowest excited $^2E(D_3)$ state as a function of the trigonal splitting. $n(a_1)$ represents the occupation number of the unique a_1 orbital; $\bar{n}(e)$ is the average occupation number of the e_θ and e_ϵ orbitals. The full lines were obtained for the Ψ wave functions, which result from a full diagonalization of the 3 × 3 interaction matrix in eq 18 with the parameter values D = 7000 cm^{-1} and D' = 700 cm^{-1}. The dashed lines refer to the occupation numbers for the approximate Ψ^0 functions, which are obtained if D' is put equal to zero (cf. eq 22). Exactly as in Figure 2 the symmetry lowering of the ligand field and the corresponding splitting of the t_{2g} shell are seen to cause a charge flow into the orbitals at lowest energy. Hence, in the case of $Cr(acac)_3$ with $\Delta\tau_2 > 0$ one predicts increased occupation of the a_1 orbital, while the opposite trend should be observed for $Cr(bpy)_3^{3+}$ with $\Delta\tau_2 < 0$.

For extremely high trigonal fields β will approach its limiting value of −1 (for $\Delta\tau_2 \to -\infty$) and +1 (for $\Delta\tau_2 \to +\infty$). It should be kept in mind that the functions in eq 20 are only valid if D' is close to zero as compared to $\Delta\tau_2$. Calculations indeed confirm that for strong trigonal fields the Ψ^0 functions provide us with reasonable approximations for the lowest energy wave vectors. However, in the vicinity of the octahedral starting point D' can certainly not be neglected as compared to $\Delta\tau_2$. Nor will the Ψ^0 functions be reliable trial functions under these coupling conditions. This point will be further discussed in the next paragraph in connection with the trigonal orbital occupation numbers.

IIIc. Orbital Occupation Numbers. The orbital composition of the lowest emitting level in trigonal d^3 complexes may be obtained by a straightforward orbital population analysis of the relevant Ψ functions. The results of such an analysis, based on representative values for D and D', are shown in Figure 6. This figure is entirely analogous to Figure 2 in the preceding section and demonstrates the charge redistribution between the trigonal t_{2g} orbitals, a_1 and e, as a result of increasing trigonal perturbation. Again the occupation number of the lower lying orbitals will be greater than 1, while the higher lying orbitals will have occupation numbers less than 1. For a complex such as $Cr(acac)_3$, which is characterized by a positive trigonal splitting, charge is expected to accumulate in the a_1 orbital at the expense of the population of the e orbitals. Precisely the opposite charge flow should occur in the tris(bipyridyl) complex, which presumably contains a negative trigonal splitting. For comparison the figure also displays approximate orbital occupation curves, which correspond to the a_1 and e populations in the Ψ^0 trial functions, given in eq 20. For these states the orbital composition as a function of the trigonal mixing coefficient β is given by

$$\Psi_\theta^0: \quad n(a_1) = 1 + 2\beta/(1 + \beta^2) \quad n(e_\theta) = 1 \quad n(e_\epsilon) = 1 - 2\beta/(1 + \beta^2) \tag{22a}$$

$$\Psi_\epsilon^0: \quad n(a_1) = 1 + 2\beta/(1 + \beta^2) \quad n(e_\theta) = 1 - 2\beta/(1 + \beta^2) \quad n(e_\epsilon) = 1 \tag{22b}$$

$$\Psi_\theta^0 \text{ or } \Psi_\epsilon^0: \quad \bar{n}(e) = \tfrac{1}{2}[n(e_\theta) + n(e_\epsilon)] = 1 - \beta/(1 + \beta^2)$$

These relations precisely parallel the corresponding quadrate expressions for the Φ functions, given in eq 8.

It should be kept in mind that the present Ψ^0 functions are only approximate wave vectors, which are not reliable near the octahedral origin. Nevertheless, the expressions in eq 22 perform reasonably well, as may be judged from Figure 6.

IIId. Discussion. All trigonal d^3 complexes have been shown to belong to only one emission class, which is characterized by an unequal orbital occupation of the trigonal t_{2g} orbitals. In consequence all trigonal emitters are expected to exhibit the characteristic spectral features, such as band broadening and solvent shifts, which in the study of Forster et al.[1] were associated with the ^2T emission class of strongly perturbed tetragonal complexes. The prominence of these effects will be proportional to the degree of charge anisotropy in the emitting state and thus will depend on the trigonal field strength as shown in Figure 6. For very weak trigonal fields, such as in the tris(ethylenediamine) complex, emission will of course still be matching the octahedral pattern, but even moderate trigonal fields should already give rise to observable effects. These predictions seem to meet Endicott's working hypothesis[24] that ligands with a tendency toward trigonal distortions might facilitate excited-state relaxation.

Broad absorption spectra and Stokes-shifted phosphorescence have certainly been observed for the $Cr(acac)_3$ compound in the crystalline study of Armendarez and Forster.[25] This spectral broadening is to a large extent due to solid-state interactions. In dilute matrices at temperatures below 10 K the $Cr(acac)_3$ emission spectrum is very narrow with the preponderance of the emission in the 0–0 bands,[26] but even under these circumstances many vibrational sidebands are present, indicating excited-state distortions. Hence, in $Cr(acac)_3$ the lowest electronic transition, with a band origin around 12 880 cm^{-1}, must be assigned to a ^2E state, of mixed ^2E_g, $^2T_{1g}$, and $^2T_{2g}$ parentage. In principle the vector composition of this state and the sign of the trigonal splitting can be obtained by Zeeman spectroscopy. However, so far such measurements have not resulted in conclusive assignments.[27]

For $Cr(bpy)_3^{3+}$ one expects on the basis of the Orgel effect a pronounced depletion of the a_1 orbital, which should be higher in energy than the e orbitals. In view of the angular form of the a_1 orbital as depicted in Figure 3, this charge flow should promote solvent attack along the direction of the threefold axis and eventually give rise to a photosubstitution reaction. Apparently this trigonal polarization must be quite pronounced since $Cr(bpy)_3^{3+}$ is one of the only Cr(III) complexes that is claimed to have a photoreactive doublet state.[28,29] Although the spectral reports of König and Herzog[30] do suggest a strong trigonal splitting for $Cr(bpy)_3^{3+}$, conclusive spectral evidence again is still lacking. Hopefully these issues can be clarified. The outcome of such studies may also necessitate a reassignment of the phosphorescent states[31] in Cr(III) tris(diimine) complexes.

The I^* bonding model, which was applied to tetragonal emitters in the previous section, can also be used to predict excited-state geometries in trigonal emitters. Here such calculations will not be pursued since no detailed empirical information with regard to the excited-state geometries in trischelated complexes is available. It should be pointed out though that, because of bidentate strain effects, excited-state charge redistributions in chelated complexes may not only affect the bond lengths but could also induce changes of the bite angles and the trigonal twist angle.

Acknowledgment. A.C. is indebted to the Belgian National Science Foundation (NFWO) for a research grant.

IV. Appendix

In this Appendix we collect some useful parameter values for typical Cr(III) complexes. Racah's interelectronic repulsion parameters B and C were taken to be $B = 700$ cm^{-1} and $C = 4B$. The calculations of the orbital occupation numbers were based on the following values for the energy gaps between the doublet levels: $D(^2T_{2g} \leftrightarrow {}^2T_{1g}) = 7000$ cm^{-1}, $D'(^2T_{1g} \leftrightarrow {}^2E_g) = 700$ cm^{-1}.

AOM parameters for various ligands coordinated at the Cr(III) ion may be found in ref 15. As an example for the fluoride ligand one has $\sigma_F \approx 7630$ cm^{-1} and $\pi_F = 1880$ cm^{-1}. For the $acac^-$ ligand we assume that $\pi_\perp(\chi)$ is almost negligible while $\pi_\perp(\psi) \approx 1000$ cm^{-1}. For the bpy ligand no parameter values could be obtained.

(24) Endicott, J. F.; Lessard, R. B.; Lei, Y.; Ryu, C. K.; Tamilarasan, R. In *Excited States and Reactive Intermediates*; Lever, A. B. P., Ed.; ACS Symposium Series 307; American Chemical Society: Washington, DC, 1986; p 85.
(25) Armendarez, P. X.; Forster, L. S. *J. Chem. Phys.* **1964**, *40*, 273.
(26) Schönherr, T.; Eyring, G.; Linder, R. *Z. Naturforsch., A: Phys., Phys. Chem., Kosmophys.* **1983**, *38A*, 736.
(27) Field, R. A.; Haidl, E.; Winscom, C. J.; Kahn, Z. H.; Plato, M.; Möbius, K. *J. Chem. Phys.* **1984**, *80*, 3082.
(28) Maestri, M.; Bolletta, F.; Moggi, L.; Balzani, V.; Henry, M. S.; Hoffman, M. Z. *J. Am. Chem. Soc.* **1978**, *100*, 2694.
(29) Jamieson, M. A.; Serpone, N.; Hoffman, M. Z. *Coord. Chem. Rev.* **1981**, *39*, 121.
(30) König, E.; Herzog, S. *J. Inorg. Nucl. Chem.* **1970**, *32*, 585.
(31) Kane-Maguire, N. A. P.; Conway, J.; Langford, C. H. *J. Chem. Soc., Chem. Commun.* **1974**, 801.

Contribution from Rocketdyne, A Division of Rockwell International, Canoga Park, California 91303

Bromine Nitrates

William W. Wilson and Karl O. Christe*

Received December 24, 1986

The reaction of BrF_5 with a large excess of $LiNO_3$ at 0 °C produces LiF, $BrONO_2$, N_2O_5, and O_2 as the principal products. The infrared spectra of $BrONO_2$ in the gas and solid phases and in N_2 and Ne matrices and the Raman spectrum of the solid phase were recorded. With the exception of the N–OBr torsional mode, all fundamental vibrations of $BrONO_2$ can be assigned and support a planar structure for this molecule. The fundamental vibrations involving the NO_2 group exhibit pronounced frequency shifts on going from the gas to the solid, indicating association in the solid phase. With N_2O_5 the $BrONO_2$ molecule forms an unstable adduct, which was shown by Raman spectroscopy to possess the ionic structure $NO_2^+[Br(ONO_2)_2]^-$. On the basis of a comparison of our results with those found in the literature and in three unpublished dissertations, it is concluded that the previously reported compounds $BrO_2 \cdot 3NO_2$, $Br(NO_3)_3$, and $BrNO_3 \cdot N_2O_5$ are all identical with our material and therefore must be assigned the composition $NO_2^+[Br(ONO_2)_2]^-$. For comparison, $Cs^+[Br(ONO_2)_2]^-$ was also prepared, and its vibrational spectra were recorded and assigned.

Introduction

In a recent study from our laboratory it was shown that the reactions of an excess of BrF_5 with the nitrates of Na, K, Rb, and Cs provide simple, high-yield, one-step syntheses for the corresponding BrF_4O^- salts and FNO_2. Since lithium does not form a stable BrF_4O^- salt, the use of $LiNO_3$ as a starting material in the above reaction afforded a direct, one-step synthesis of BrF_3O.[1] During the study of the $LiNO_3$–BrF_5 system, it was found that

(1) Wilson, W. W.; Christe, K. O. *Inorg. Chem.* **1987**, *26*, 916.

0020-1669/87/1326-1573$01.50/0